Ten Years of Gabor-Domain Optical Coherence Microscopy

Cristina Canavesi[1,*], **Jannick P. Rolland**[1,2]

[1]LighTopTech Corp., 150 Lucius Gordon Drive, Suite 201, West Henrietta, NY 14586-9687, USA;

[2]The Institute of Optics, University of Rochester, Rochester, NY 14627, USA

Abstract

Gabor-domain optical coherence microscopy (GDOCM) is a high-definition imaging technique leveraging principles of low-coherence interferometry, liquid lens technology, high-speed imaging, and precision scanning. GDOCM achieves isotropic 2 μm resolution in 3D, effectively breaking the cellular resolution limit of optical coherence tomography (OCT). In the ten years since its introduction, GDOCM has been used for cellular imaging in 3D in a number of clinical applications, including dermatology, oncology and ophthalmology, as well as to characterize materials in industrial applications. Future developments will enhance the structural imaging capability of GDOCM by adding functional modalities, such as fluorescence and elastography, by estimating thicknesses on the nano-scale, and by incorporating machine learning techniques.

Keywords

optical coherence tomography; noninvasive imaging; Gabor-domain optical coherence microscopy

1. Introduction

Histopathology, the gold standard for diagnosis at the cellular level, suffers from morbidity, cost, and time associated with a biopsy; overcoming these limitations with optical biopsy is the holy grail. The capability to noninvasively image the cellular structures in real-time will revolutionize medicine. The requirements for optical biopsy include cellular resolution (<5 μm) in 3D, 1 mm^2 field of view, and depth of imaging of at least 1 mm in tissue. Real-time operation is desired.

2. Strategies for Cellular-Resolution Imaging

Noninvasive imaging techniques, which include ultrasound, optical coherence tomography (OCT), and confocal microscopy, are routinely used in clinical applications for providing insight on tissue structural morphology These methods face a tradeoff between spatial resolution and depth of imaging, as depicted in Figure 1, in which the application space is shown in log-scale for the two key parameters of transverse resolution and imaging depth.

*Correspondence: cristina@lightoptech.com.

Conflicts of Interest: The authors are co-founders and President (C.C.) and CTO (J.P.R.) of LighTopTech Corp.

These two parameters determine what kind of features can be imaged—including cellular and subcellular—and at what depth inside of the tissue. With typical cellular structures having a size of 10–20 μm, a resolution <5 μm is desired to visualize the cellular morphology A depth of imaging of ~1 mm or more is advantageous to track cellular changes in tissue induced by various diseases.

OCT is an optical imaging technique based on low-coherence interferometry with an axial resolution on the micrometer-scale and lateral resolution limited to tens of micrometers [2], OCT produces cross-sectional views of tissue up to a depth of several millimeters. In OCT, transverse and axial resolutions are decoupled. OCT—in particular spectral domain OCT (SD-OCT)—is widely used in ophthalmic and cardiovascular applications [2,3].

Confocal microscopy, with micron or submicron lateral resolution, has depth of imaging limited to tens of micrometers [4]. Optical imaging system, including OCT and confocal microscopy, face a trade-off between lateral resolution and depth of imaging. To increase the lateral resolution x, the numerical aperture (NA) is increased, resulting in shallower depth of focus (DOF), as illustrated in Figure 2.

Optical coherence microscopy (OCM) was introduced as a variant of OCT to achieve micrometer-scale resolution [5]. OCM uses a higher NA objective (i.e., ~0.2) than conventional OCT (i.e., ~0.04), and can produce cellular imaging at the expense of a reduction in depth of focus (100–200 μm). OCM variants include point-canning OCM and full-field OCM [6–8]. In full-field OCM, more often referred to as full-field OCT (FF-OCT), en face images are acquired. Computational approaches for extending the depth of focus in OCM have been proposed successfully [9,10].

The choice of the light source in OCT and OCM has direct impact on both transverse and axial resolutions, as well as on imaging depth, since transverse resolution is linearly proportional to the central wavelength, axial resolution is inversely proportional to the bandwidth, and longer wavelengths penetrate deeper into tissue. Superluminescent diodes (SLDs) [11] are broadly used in OCT due to availability in the 800,1300, and 1500 nm spectral bands, relatively large bandwidth (typically 50–100 nm), affordability, and increased brightness (at the expense of bandwidth) over thermal sources [12], An advantage of fluorescence-based sources, which have been employed in FF-OCT in conjunction with pulsed illumination to reduce motion artifacts, is the smoothness of the spectrum, yet their applicability is limited due to cost and requirement of a high-power laser excitation source [13]. Light-emitting diodes (LEDs), have been described to produce submicron axial resolution in FF-OCT with spatial resolution and sensitivity equivalent to those obtained with halogen sources [14]. Supercontinuum sources offer ultrawide bandwidths (more than 1000 nm) and brightness an order of magnitude greater than SLDs, but are still more expensive than SLDs [15]. Yet, they provide superior precision in a thickness estimation task [16,17]. Advances in swept sources have led OCT to achieve multi-MHz acquisition speeds [18], while at the same time they often suffer from jitter that may cause significant uncertainty in a class thickness estimation task [16]. To date, visible light OCT mainly employs spatially coherent light sources, however broadband spatially incoherent light sources have been demonstrated successfully [19].

3. Gabor-Domain Optical Coherence Microscopy

Gabor-domain optical coherence microscopy (GDOCM) is a high transverse resolution variant of spectral domain optical coherence tomography (SD-OCT) [20]. A schematic of the GDOCM system is shown in Figure 3.

In GDOCM, the choice of wavelength range in the near infrared was made prioritizing lateral resolution over imaging depth and penetration into tissue. The light source is a superluminescent diode with a center wavelength of 840 nm and 100 nm bandwidth, yielding axial resolution of 3.1 μm in air and 2 μm in tissue (at a refractive index of 1.3). A 50:50 fiber coupler is used for the interferometer. The reference arm performs optical path length matching and dispersion compensation by incorporating a dispersive element [21]. Polarization controllers are used to maximize fringe interference by matching the polarization of the light in the two arms of the interferometer. Optionally, the dispersion and polarization adjustments can be performed to compensate changes in dispersion and polarization introduced by the sample itself. The spectral interference signal is acquired at a line rate of 80 kHz, with imaging depth in the sample greater than 2 mm with a custom Czerny-Turner spectrometer, which includes a reflective dispersive element and a line camera with CMOS (complementary metal oxide semiconductor) sensor. The spectrometer design eliminates coma by incorporating two off-axis spherical mirrors, and a cylindrical lens is used to compensate astigmatism in the beam introduced by the off-axis mirrors [22]. A 2 μm transverse resolution is achieved over a field of view of 2×2 mm in the GDOCM microscope design with a numerical aperture of 0.2, with experimental depth of focus of ~100 μm [23]. A compact dual-axis MEMS (microelectromechanical system) mirror integrated in the microscope is used to scan the beam over the 2D field of view [24]. The microscope can be operated in two modalities, to be selected for the desired application: In contact with the sample (with gel medium to create optical contact between the distal surface of the microscope and the sample), or with a working distance of 15 mm. The contact imaging modality may be more advantageous to maximize signal collection in highly scattering tissues such as skin, while the 15 mm working distance is preferred for ophthalmic applications, or for imaging areas that are more difficult to reach with a contact probe, such as certain locations on the face. In order to obtain micron-resolution imaging over the entire volume, multiple volumetric images of the sample (termed zones) are acquired, each corresponding to a different focusing; depth. A good rule of thumb for the number of zones to be acquired is to consider the ratio between total sample depth and the depth of focus; for example, given the depth of focus of ~100 μm, for a total sample depth of 600 μm, six zones are required. A liquid lens integrated in the optical design of thief microscope achieves dynamic refocusing with no moving parts over a 2 mm range [25]. The in-focus portions of each volumetric zone are extracted and merged together to produce a high-definition volume with invariant 2 μm resolution, both axially and transversally. The process of combining together the in-focus portions of the zones is referred to as fusing. Fusing can be performed either in the spatial or spectral domains [26,27]. as example of a GDOCM image of a human fingertip acquired with three zones and the corresponding fusing procedure is shown in Figure 4.

Parallel processing of the acquired data on graphics processing units (GPUs) achieves near real-time visualization of the volumetric images [28].

The 2015 and 2018 implementations of GDOCM are shown in Figure 5. A standalone cart houses the entire GDOCM system. While the first prototype shown in Figure 5a included several elements mounted on a breadboard assembly, the instrument shown in Figure 5b was entirely re-engineered with precision mechanics for robust and reliable operation, and incorporates a custom software for semiautomated image acquisition, and 3D image visualization and analysis.

The microscope can be operated either as a handheld or with an articulated arm (see Figure 6, for an example of contact mode with a mechanical arm). The use of a mechanical arm is desired to minimize motion artifacts introduced by operator hand tremor.

A comparison of the imaging performance of confocal microscopy, spectral domain optical coherence tomography, optical coherence microscopy, full-field optical coherence tomography, and Gabor-domain optical coherence microscopy is reported in Table 1. The performance of the various imaging modalities relates to the chart in Figure 1, with SD-OCT suffering from limited transverse resolution while offering excellent imaging depth of several millimeters, while confocal microscopy, OCM, and FF-OCT achieve subcellular resolution over a limited imaging depth. GDOCM balances these parameters to achieve cellular resolution over an imaging depth of 2 mm. SD-OCT, OCM, and GDOCM, being spectral domain OCT systems, have a cross-sectional image orientation, while CM and FF-OCT (time domain OCT) have an en face image orientation. A main limitation of confocal microscopy, unlike OCT, is that the sectioning in depth is set by the NA of the objective lens. Contact operation is typically required with clinical confocal microscopes, however contactless implementations have been proposed. Higher sectioning is obtained with higher NA, yet this occurs at the expense of DOF. Because axial sectioning in OCT is independent of the NA, since it is set by the spectral bandwidth, both higher axial sectioning and larger DOF are possible with OCT. Furthermore, it may be difficult to assess the depth of imaging with confocal, as only en face planes are acquired. SD-OCT acquires depth scans, from which the volume is assembled, and the depth of any en face plane is directly acquired from the depth scan. While the methods that offer higher transverse resolution typically have limited FOV, mosaicing is often used to provide wide FOV imaging, naturally at the expense of acquisition time.

4. Applications

Originally developed for ophthalmic applications to image the posterior segment of the eye [3,33–35] and further enhanced with OCT angiography [36,37], OCT has found successful applications in the anterior segment of the eye [30], as well as in a number of fields, including dermatology [38,39], oncology [40–46] and dentistry [47]; in endoscopic form it has been applied to cardiology [48,49], gastroenterology [50,51], and pulmonology [52–54]. Numerous embodiments of functional OCT [55], including Doppler OCT and polarization-sensitive OCT [56,57], as well as optical coherence elastography [58–64], multimodal

fluorescence-OCT [2,65–67] and spectroscopic OCT [68], have been developed to enhance the structural information obtained with OCT with properties related to tissue function.

To date, GDOCM has been used in a number of medical applications, including human skin ex vivo [69,70] and in vivo [71], human corneas ex vivo [72], mouse cornea in vivo, and cervical tissue ex vivo [73], as well as industrial applications [74,75]. When reviewing the images, having access to the 3D views offers additional insights into tissue morphology; the en face views are useful to visualize cellular structures. Representative images of human skin, cornea, and cervical tissue are shown in Figure 7. The depth cross-sections can be directly related to traditional histology slices, since they are presented in the same orientation. The en face views, which are in the traditional orientation of microscopy, including confocal microscopy, highlight the presence of cellular structures, including endothelial cells (Figure 7b, bottom) and corneal nerves (Figure 7c, bottom). Various diseases that cause disruption of the cellular network, such as basal cell carcinoma (BCC) and cervical dysplasia, can be assessed, such as in Figure 7a,d. Various measurements can be conducted on the 3D GDOCM images to extract relevant parameters, such as quantifying the thicknesses of various sublayers of the tissue, and estimating the cell density [76].

5. Conclusions

A number of developments are under course to further enhance the cellular-resolution imaging capabilities of GDOCM. These include applying machine learning to automatically segment features of interest of the image; adding functional capabilities to enhance GDOCM′s structural imaging at the microscopic level, such as fluorescence and elastography; and thickness estimation of nano-scale layers.

Funding:

References

1. Fujimoto JG Optical Coherence Tomography: Introduction In Handbook of Optical Coherence Tomography; Bouma BE, Tearney GJ, Eds.; Taylor & Francis: Boca Raton, FL, USA, 2001; ISBN 9781420002508.

2. Drexler W; Liu M; Kumar A; Kamali T; Unterhuber A; Leitgeb RA Optical coherence tomography today: Speed, contrast, and multimodality. J. Biomed. Opt 2014, 19, 71412.

3. Zysk AM; Nguyen FT; Oldenburg AL; Marks DL; Boppart SA Optical coherence tomography: A review of clinical development from bench to bedside. J. Biomed. Opt 2007, 12, 051403. [PubMed: 17994864]

4. Minsky M Microscopy Apparatus. U.S. Patent 3,013,467, 19 12 1961.

5. Aguirre AD; Hsiung P; Ko TH; Hartl I; Fujimoto JG High-resolution optical coherence microscopy for high-speed, in vivo cellular imaging. Opt. Lett 2003, 28, 2064–2066. [PubMed: 14587816]

6. Dubois A; Grieve K; Moneron G; Lecaque R; Vabre L; Boccara C Ultrahigh-resolution full-field optical coherence tomography. Appl. Opt 2004, 43, 2874–2883. [PubMed: 15143811]

7. Leitgeb RA En face optical coherence tomography: A technology review. Biomed. Opt. Express 2019, 10, 2177–2201. [PubMed: 31143489]

8. Thouvenin O; Grieve K; Xiao P; Apelian C; Boccara AC En face coherence microscopy. Biomed. Opt. Express 2017, 8, 622–639. [PubMed: 28270972]

9. Ralston TS; Marks DL; Carney PS; Boppart SA Interferometric synthetic aperture microscopy. Nat. Phys 2007, 3, 129–134. [PubMed: 25635181]

10. Ahmad A; Shemonski ND; Adie SG; Kim H-S; Hwu W-MW; Carney PS; Boppart SA Real-time in vivo computed optical interferometric tomography. Nat. Photonics 2013, 7, 444–448. [PubMed: 23956790]

11. Shidlovski VR Superluminescent diode light sources for OCT In Optical Coherence Tomography: Technology and Applications, 2nd ed.; Drexler W, Fujimoto JG, Eds.; Springer: Cham, Switzerland, 2015; ISBN 9783319064192.

12. Fercher AF; Hitzenberger CK; Sticker M; Moreno-Barriuso E; Leitgeb R; Drexler W; Sattmann H Thermal light source technique for optical coherence tomography. Opt. Commun 2000, 185, 57–64.

13. Sacchet D; Brzezinski M; Moreau J; Georges P; Dubois A Motion artifact suppression in full-field optical coherence tomography. Appl. Opt 2010, 49, 1480–1488. [PubMed: 20300141]

14. Ogien J; Dubois A High-resolution full-field optical coherence microscopy using a broadband light-emitting diode. Opt. Express 2016, 24, 9922–9931. [PubMed: 27137603]

15. Froehly L; Meteau J Supercontinuum sources in optical coherence tomography: A state of the art and the application to scan-free time domain correlation techniques and depth dependant dispersion compensation. Opt. Fiber Technol 2012, 18, 411–419.

16. Huang J; Yao J; Cirucci N; Ivanov T; Rolland JP Performance analysis of optical coherence tomography in the context of a thickness estimation task Jinxin Huang tomography in the context of a thickness. J. Biomed. Opt 2015, 20, 121306. [PubMed: 26378988]

17. Huang J; Hindman HB; Rolland JP In vivo thickness dynamics measurement of tear film lipid and aqueous layers with optical coherence tomography and maximum-likelihood estimation. Opt. Lett 2016, 41, 1981–1984. [PubMed: 27128054]

18. Klein T; Huber R High-speed OCT light sources and systems. Biomed. Opt. Express 2017, 8, 828–859. [PubMed: 28270988]

19. Shu X; Beckmann L; Zhang HF Visible-light optical coherence tomography: A review. J. Biomed. Opt 2017, 22, 121707.

20. Rolland JP; Meemon P; Murali S; Jain A; Papp N; Thompson KP; Lee K-S Gabor domain optical coherence microscopy In Proceedings of the 1st Canterbury Workshop on Optical Coherence Tomography and Adaptive Optics, Proceedings of SPIE, Canterbury, UK, 30 12 2008; Podoleanu AG, Ed.; Volume 7139, p. 71390F.

21. Lee K-S; Akcay AC; Delemos T; Clarkson E; Rolland JP Dispersion control with a Fourier-domain optical delay line in a fiber-optic imaging interferometer. Appl. Opt 2005, 44, 4009–4022. [PubMed: 16004048]

22. Lee K-S; Thompson KP; Rolland JP Broadband astigmatism-corrected Czerny-Turner spectrometer. Opt. Express 2010, 18, 23378–23384. [PubMed: 21164679]

23. Murali S; Meemon P; Lee K-S; Kuhn WP; Thompson KP; Rolland JP Assessment of a liquid lens enabled in vivo optical coherence microscope. Appl. Opt 2010, 49, D145–D156. [PubMed: 20517356]

24. Cogliati A; Canavesi C; Hayes A; Tankam P; Duma V-F; Santhanam A; Thompson KP; Rolland JP MEMS-based handheld scanning probe with pre-shaped input signals for distortion-free images in Gabor-Domain Optical Coherence Microscopy. Opt. Express 2016, 24, 13365–13374. [PubMed: 27410354]

25. Murali S; Thompson KP; Rolland JP Three-dimensional adaptive microscopy using embedded liquid lens. Opt. Lett 2009, 34, 145–147. [PubMed: 19148236]

26. Rolland JP; Meemon P; Murali S; Thompson KP; Lee K Gabor-based fusion technique for Optical Coherence Microscopy. Opt. Express 2010, 18, 3632–3642. [PubMed: 20389373]

27. Meemon P; Widjaja J; Rolland JP Spectral fusing Gabor domain optical coherence microscopy. Opt. Lett 2016, 41, 508–511. [PubMed: 26907410]

28. Tankam P; Santhanam AP; Lee K-S; Won J; Canavesi C; Rolland JP Parallelized multi–graphics processing unit framework for high-speed Gabor-domain optical coherence microscopy. J. Biomed. Opt 2014, 19, 71410. [PubMed: 24695868]

29. Zhivov A; Stachs O; Stave J; Guthoff RF In vivo three-dimensional confocal laser scanning microscopy of corneal surface and epithelium. Br. J. Ophthalmol 2009, 93, 667. [PubMed: 18650213]

30. Ang M; Baskaran M; Werkmeister RM; Chua J; Schmidl D; Aranha dos Santos V; Garhöfer G; Mehta JS; Schmetterer L Anterior segment optical coherence tomography. Prog. Retin. Eye Res 2018, 66, 132–156. [PubMed: 29635068]

31. Tan B; Hosseinaee Z; Han L; Kralj O; Sorbara L; Bizheva K 250 kHz, 1.5 um resolution SD-OCT for in-vivo cellular imaging of the human cornea. Biomed. Opt. Express 2018, 9, 6569–6583. [PubMed: 31065450]

32. Mazlin V; Xiao P; Dalimier E; Grieve K; Irsch K; Sahel J-A; Fink M; Boccara AC In vivo high resolution human corneal imaging using full-field optical coherence tomography. Biomed. Opt. Express 2018, 9, 557–568. [PubMed: 29552393]

33. Fujimoto J; Swanson E The development, commercialization, and impact of optical coherence tomography. Investig. Ophthalmol. Vis. Sci 2016, 57, OCT1–OCT13. [PubMed: 27409459]

34. Vakoc BJ; Fukumura D; Jain RK; Bouma BE Cancer imaging by optical coherence tomography— Preclinical progress and clinical potential. Nat. Rev. Cancer 2012, 12, 363–368. [PubMed: 22475930]

35. Drexler W; Fujimoto JG State-of-the-art retinal optical coherence tomography. Prog. Retin. Eye Res 2008, 27, 45–88. [PubMed: 18036865]

36. Spaide RF; Fujimoto JG; Waheed NK; Sadda SR; Staurenghi G Optical coherence tomography angiography. Prog. Retin. Eye Res 2018, 64, 1–55. [PubMed: 29229445]

37. Kashani AH; Chen CL; Gahm JK; Zheng F; Richter GM; Rosenfeld PJ; Shi Y; Wang RK Optical coherence tomography angiography: A comprehensive review of current methods and clinical applications. Prog. Retin. Eye Res 2017, 60, 66–100. [PubMed: 28760677]

38. Gambichler T; Pljakic A; Schmitz L Recent advances in clinical application of optical coherence tomography of human skin. Clin. Cosmet. Investig. Dermatol 2015, 8, 345–354.

39. Olsen J; Holmes J; Jemec GBE Advances in optical coherence tomography in dermatology—A review. J. Biomed. Opt 2018, 23, 040901.

40. Wilder-Smith P; Krasieva T; Jung W-G; Zhang J; Chen Z; Osann K; Tromberg B Noninvasive imaging of oral premalignancy and malignancy. J. Biomed. Opt 2005, 10, 051601. [PubMed: 16292949]

41. Escobar PF; Rojas-Espaillat L; Tisci S; Enerson C; Brainard J; Smith J; Tresser NJ; Feldchtein FI; Rojas LB; Belinson JL Optical coherence tomography as a diagnostic aid to visual inspection and colposcopy for preinvasive and invasive cancer of the uterine cervix. Int. J. Gynecol. Cancer 2006, 16, 1815–1822. [PubMed: 17009977]

42. Gallwas J; Jalilova A; Ladurner R; Kolben TM; Kolben T; Ditsch N; Homann C; Lankenau E; Dannecker C Detection of cervical intraepithelial neoplasia by using optical coherence tomography in combination with microscopy. J. Biomed. Opt 2017, 22, 16013. [PubMed: 28118427]

43. Assayag O; Grieve K; Devaux B; Harms F; Pallud J; Chretien F; Boccara C; Varlet P Imaging of non-tumorous and tumorous human brain tissues with full-field optical coherence tomography. NeuroImage Clin. 2013, 2, 549–557. [PubMed: 24179806]

44. Nguyen FT; Zysk AM; Chaney EJ; Kotynek JG; Oliphant UJ; Bellafiore FJ; Rowland KM; Johnson PA; Boppart SA Intraoperative evaluation of breast tumor margins with optical coherence tomography. Cancer Res. 2009, 69, 8790–8796. [PubMed: 19910294]

45. Betz CS; Volgger V; Silverman SM; Rubinstein M; Kraft M; Arens C; Wong BJF Clinical optical coherence tomography in head & neck oncology: Overview and outlook. Head Neck Oncol. 2013, 5, 35.

46. Wang J; Xu Y; Boppart SA Review of optical coherence tomography in oncology. J. Biomed. Opt 2017, 22, 121711.

47. Machoy M; Seeliger J; Szyszka-Sommerfeld L; Koprowski R; Gedrange T; Wo niak K The Use of Optical Coherence Tomography in Dental Diagnostics: A State-of-the-Art Review. J. Healthc. Eng 2017, 2017.

48. Fujimoto JG; Schmitt JM; Swanson EA; Jang IK The development of OCT In Cardiovascular OCT Imaging; Springer: Cham, Switzerland, 2015; ISBN 9783319108018.

49. Bezerra HG; Costa MA; Guagliumi G; Rollins AM; Simon DI Intracoronary Optical Coherence Tomography: A Comprehensive Review. Clinical and Research Applications. JACC Cardiovasc. Interv 2009, 2, 1035–1046. [PubMed: 19926041]

50. Tearney GJ; Brezinski ME; Bouma BE; Boppart SA; Pitris C; Southern JF; Fujimoto JG In vivo endoscopic optical biopsy with optical coherence tomography. Science 1997, 276, 2037–2039. [PubMed: 9197265]

51. Tsai T-H; Leggett CL; Trindade AJ Optical coherence tomography in gastroenterology: A review and future outlook. J. Biomed. Opt 2017, 22, 121716.

52. McLaughlin RA; Yang X; Quirk BC; Lorenser D; Kirk RW; Noble PB; Sampson DD Static and dynamic imaging of alveoli using optical coherence tomography needle probes. J. Appl. Physiol 2012, 113, 967–974. [PubMed: 22773771]

53. Lorenser D; Quirk BC; Auger M; Madore W-J; Kirk RW; Godbout N; Sampson DD; Boudoux C; McLaughlin RA Dual-modality needle probe for combined fluorescence imaging and three-dimensional optical coherence tomography. Opt. Lett 2013, 38, 266–268. [PubMed: 23381406]

54. Hariri LP; Mino-Kenudson M; Lanuti M; Miller AJ; Mark EJ; Suter MJ Diagnosing lung carcinomas with optical coherence tomography. Ann. Am. Thorac. Soc 2015, 12, 193–201. [PubMed: 25562183]

55. Kim J; Brown W; Maher JR; Levinson H; Wax A Functional optical coherence tomography: Principles and progress. Phys. Med. Biol 2015, 60, R211–R237. [PubMed: 25951836]

56. de Boer JF; Hitzenberger CK; Yasuno Y Polarization sensitive optical coherence tomography—A review. Biomed. Opt. Express 2017, 8, 1838. [PubMed: 28663869]

57. Canavesi C; Morichetti F; Canciamilla A; Persia F; Melloni A Polarization- and phase-sensitive low-coherence interferometry setup for the characterization of integrated optical components. J. Light. Technol 2009, 27, 3062–3074.

58. Zvietcovich F; Rolland JP; Yao J; Meemon P; Parker KJ Comparative study of shear wave-based elastography techniques in optical coherence tomography. J. Biomed. Opt 2017, 22, 35010. [PubMed: 28358943]

59. Meemon P; Yao J; Chu Y-J; Zvietcovich F; Parker KJ; Rolland JP Crawling wave optical coherence elastography. Opt. Lett 2016, 41, 847–850. [PubMed: 26974061]

60. Sun C; Standish B; Yang VXD Optical coherence elastography: Current status and future applications. J. Biomed. Opt 2011, 16, 043001. [PubMed: 21529067]

61. Wang S; Larin KV Optical coherence elastography for tissue characterization: A review. J. Biophotonics 2015, 8, 279–302. [PubMed: 25412100]

62. Kennedy BF; Kennedy KM; Sampson DD A review of optical coherence elastography: Fundamentals, techniques and prospects. IEEE J. Sel. Top. Quantum Electron 2014, 20, 1–17.

63. Rolland JP; Zvietcovich F; Ge G; Parker KJ Perspectives and advances in optical elastography In Proceedings of the Optical Elastography and Tissue Biomechanics VI, San Francisco, CA, USA, 2–7 2 2019; Volume 10880, p. 108800G.

64. Mulligan JA; Untracht GR; Chandrasekaran SN; Brown CN; Adie SG Emerging Approaches for High-Resolution Imaging of Tissue Biomechanics with Optical Coherence Elastography. IEEE J. Sel. Top. Quantum Electron 2016, 22, 6800520.

65. Auksorius E; Bromberg Y; Motiej nait R; Pieretti A; Liu L; Coron E; Aranda J; Goldstein AM; Bouma BE; Kazlauskas A; et al. Dual-modality fluorescence and full-field optical coherence microscopy for biomedical imaging applications. Biomed. Opt. Express 2012, 3, 661–666. [PubMed: 22435110]

66. Makhlouf H; Perronet K; Dupuis G; Lévêque-Fort S; Dubois A Simultaneous optically sectioned fluorescence and optical coherence microscopy with full-field illumination. Opt. Lett 2012, 37, 1613–1615. [PubMed: 22627513]

67. Thouvenin O; Fink M; Boccara C Dynamic multimodal full-field optical coherence tomography and fluorescence structured illumination microscopy. J. Biomed. Opt 2017, 22, 26004. [PubMed: 28195601]

68. Nam HS; Yoo H Spectroscopic optical coherence tomography: A review of concepts and biomedical applications. Appl. Spectrosc. Rev 2018, 53, 91–111.

69. Lee K-S; Zhao H; Ibrahim SF; Meemon N; Khoudeir L; Rolland JP Three-dimensional imaging of normal skin and nonmelanoma skin cancer with cellular resolution using Gabor domain optical coherence microscopy. J. Biomed. Opt 2012, 17, 126006. [PubMed: 23208217]

70. Rolland JP; Lee KS; Meemon P; Ibrahim SF Gabor Domain Optical Coherence Microscopy of Human Skin In Advances in Dermatological Sciences; The Royal Society of Chemistry: London, UK, 2014; pp. 37–52. ISBN 978-1-84973-398-4.

71. Tankam P; Soh J; Canavesi C; Lanis M; Hayes A; Cogliati A; Rolland JP; Ibrahim SF Gabor-Domain Optical Coherence Tomography to Aid in Mohs Resection of Basal Cell Carcinoma. J. Am. Acad. Dermatol 2019, 80, 1766–1769. [PubMed: 30287317]

72. Tankam P; He Z; Thuret G; Hindman HB; Canavesi C; Coyoc Escudero J; Lepine T; Gain P; Rolland JP Capabilities of Gabor-domain Optical Coherence Microscopy for the Assessment of Corneal Disease. J. Biomed. Opt 2019, 24, 046002.

73. Canavesi C; O'Connell R; Pazcos T; Cogliati A; Hayes A; Bonham A; Rolland JP Gabor-domain optical coherence microscopy for optical biopsy, image-guided surgery, and intraoperative imaging. Int. J. CARS (Computer Assisted Radiology and Surgery) 2019, 14 (Suppl. 1), S18–S19.

74. Canavesi C; Cogliati A; Hayes A; Santhanam AP; Tankam P; Rolland JP Gabor-domain optical coherence microscopy with integrated dual-axis MEMS scanner for fast 3D imaging and metrology In Proceedings of the SPIE—The International Society for Optical Engineering, New York, NY, USA, 11 10 2015; Volume 9633, p. 96330O.

75. Tankam P; Won J; Canavesi C; Cox I; Rolland JP Optical Assessment of Soft Contact Lens Edge-Thickness. Optom. Vis. Sci 2016, 93, 987–996. [PubMed: 27232902]

76. Canavesi C; Cogliati A; Yoon C; Mietus A; Qi Y; Stone JJ; Hindman HB; Rolland JP 3D cellular imaging of the cornea with Gabor-domain optical coherence microscopy In Proceedings of the SPIE 10867, Optical Coherence Tomography and Coherence Domain Optical Methods in Biomedicine XXIII, San Francisco, CA, USA, 2–7 2 2019; p. 108670F.
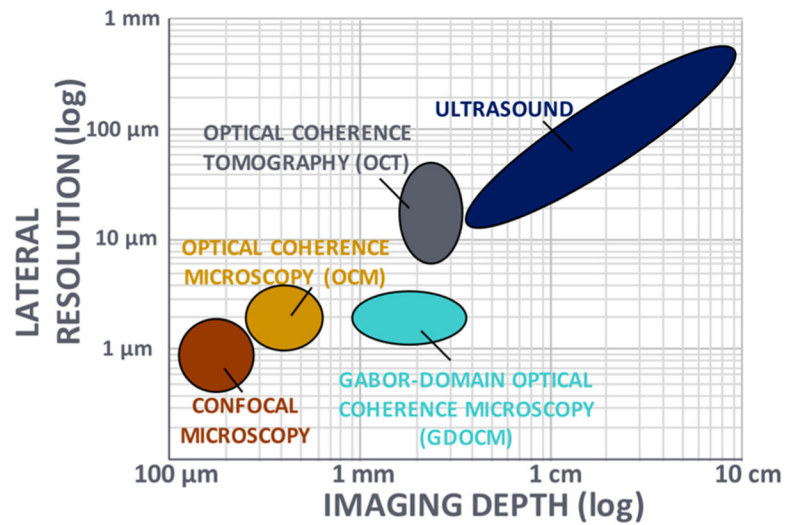
Figure 1.
Noninvasive imaging techniques (adapted from [1]). Ultrasound and optical coherence tomography suffer from insufficient lateral resolution for cellular imaging, while confocal microscopy and optical coherence microscopy suffer from limited imaging depth in tissue. Gabor-domain optical coherence microscopy was introduced to overcome the tradeoff between transverse resolution and depth of focus.
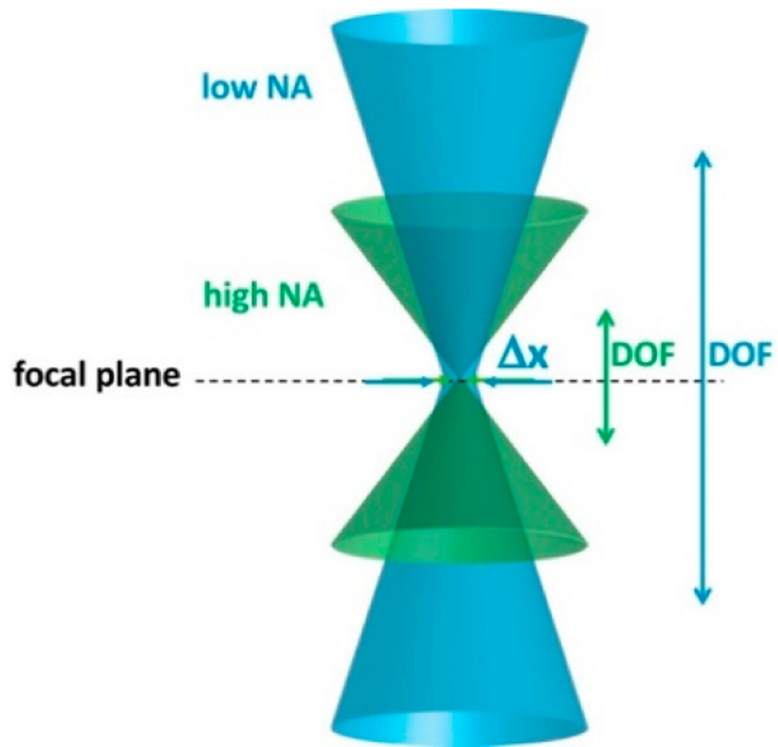
Figure 2.
Tradeoff between lateral resolution (x) and depth of focus (DOF) in an optical imaging system. NA: Numerical aperture.
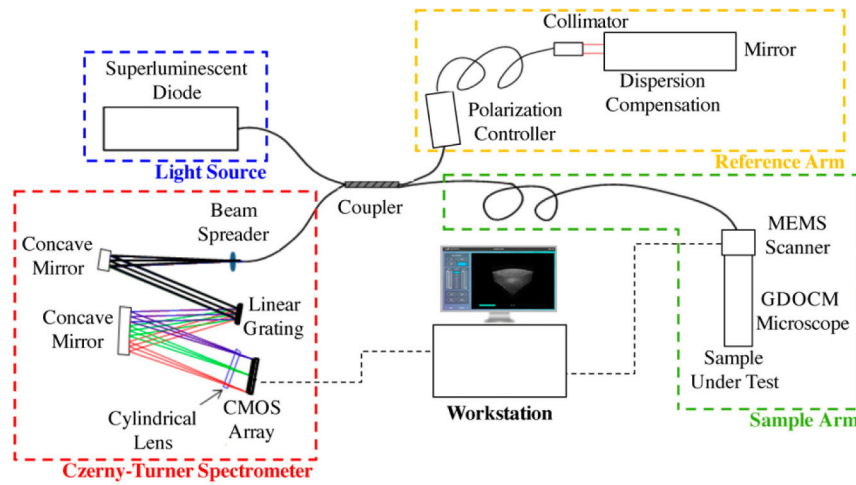
Figure 3.
Schematic of a Gabor-domain optical coherence microscopy (GDOCM) microscope consisting of a fiber-based Michelson interferometer. CMOS: Complementary metal oxide semiconductor; MEMS: Microelectromechanical systems.
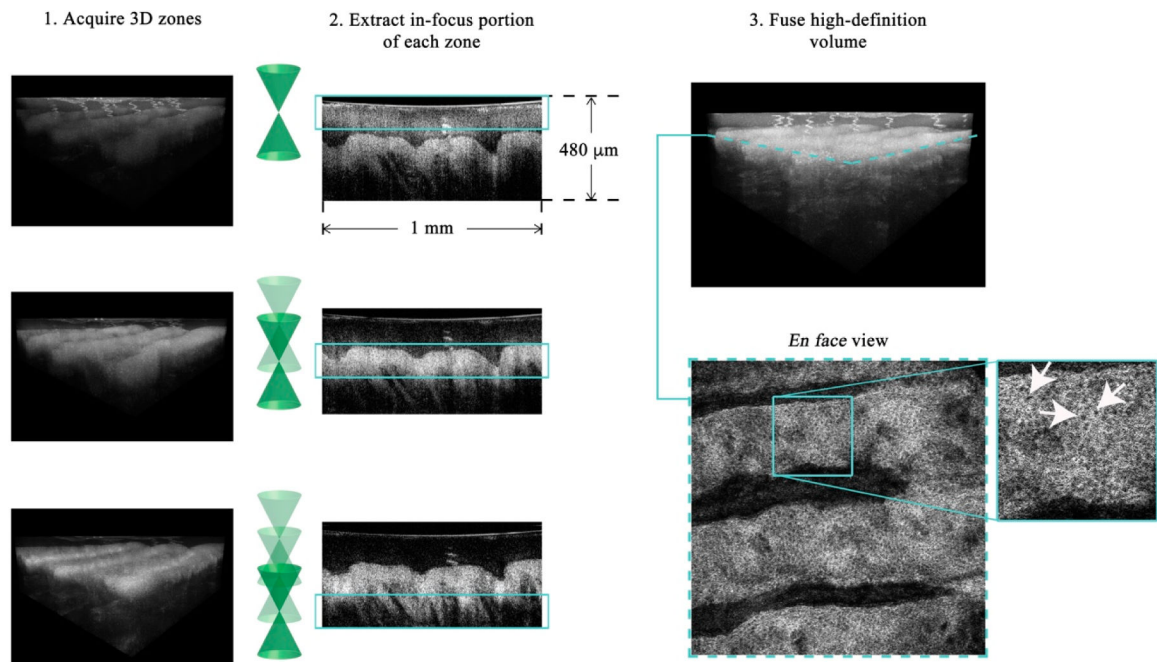
Figure 4.

Example of GDOCM image acquisition and fusing of a human fingertip. The field of view is
1×1 mm. After acquiring the desired number of zones (three in this case), the in-focus
portions are extracted and fused in a high-definition volumetric image, which achieves
cellular resolution throughout the volume. An en face view of the dermoepidermal junction
(corresponding to the dashed teal line in the 3D view), with basal cells clearly visible (white
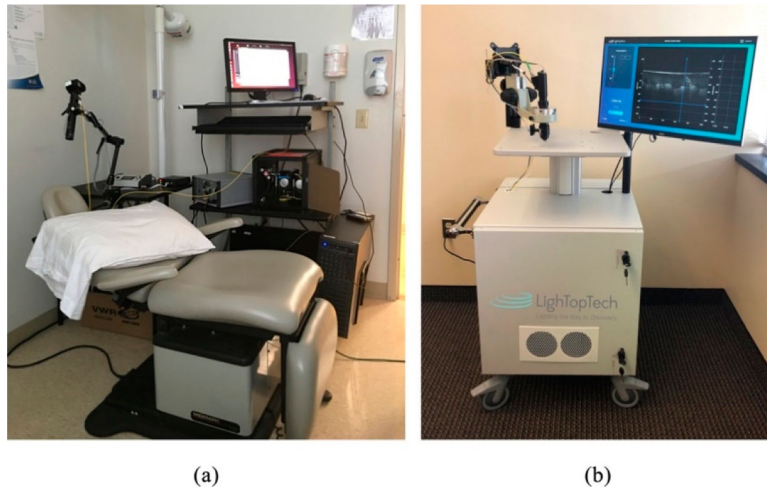arrows), is shown.

Figure 5.
(**a**) GDOCM system in use at the University of Rochester Department of Dermatology in its first in vivo study in the fall of 2015; (**b**) 2018 version of GDOCM (LighTopTech Corp. GDOCM 4D™).

Figure 6.
Handheld GDOCM microscope. A mechanical arm can be used to reduce operator hand tremor.
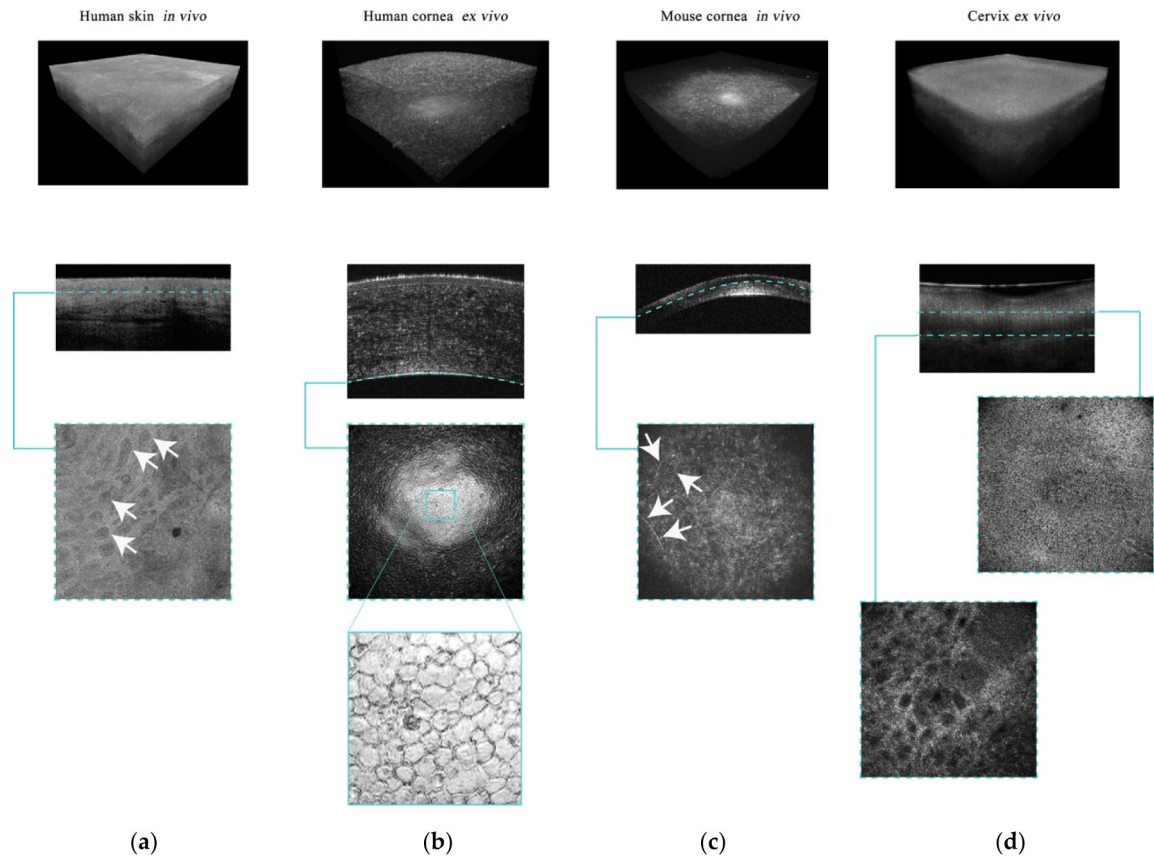
Human skin *in vivo*   Human cornea *ex vivo*   Mouse cornea *in vivo*   Cervix *ex vivo*

(**a**)   (**b**)   (**c**)   (**d**)

Figure 7.
Representative 3D, cross-sectional, and en face views for different GDOCM applications:
(**a**) In vivo human skin with basal cell carcinoma (BCC), (**b**) ex vivo human cornea, (**c**) in
vivo mouse cornea, and (**d**) ex vivo human cervical tissue. The images have a field of view
of 1×1 mm. The arrows in the en face view of in vivo human skin indicate the BCC. The en
face view of the human cornea shows the endothelium, a single layer of cells lining the
posterior surface of the cornea, with the endothelial cells clearly visible. The arrows in the
en face view of a mouse cornea acquired in vivo indicate the corneal nerves. In the images of
uterine cervix, cervical stroma, basement membrane, and cervical epithelium are visible

Table 1.

Comparison of noninvasive imaging technologies. CM: Confocal microscopy; FF-OCT: Full-field optical coherence tomography; SD-OCT: Spectral domain optical coherence tomography; OCM: Optical coherence microscopy; GDOCM: Gabor-domain optical coherence microscopy.

Technology	Axial Resolution (μm)	Transverse Resolution (μm)	Imaging Depth (mm)	Field of View (mm)	Image Orientation	Contact
CM [29]	7.6	1–2	<0.1	0.4 × 0.4	En face	Yes
SD-OCT [30]	1–10	10–20	6	6–16	Cross-sectional	No
OCM [31]	1.5	1.5	<0.2	0.8 × 0.8	Cross-sectional	Not required
FF-OCT [14,32]	0.7–7.7	1.7–2	<1	0.9–1.3 × 0.9–1.3	En face	Not required
GDOCM	2	2.6	2.5	1.5 × 1.5	Cross-sectional	Not required